Macromolecules
ARTICLE

Macromolecules **2010**, *43*, 6789–6799 **6789**
DOI: 10.1021/ma1012122

Rheology and Structure of Molten, Olefin Multiblock Copolymers

Heon E. Park and John M. Dealy*

Department of Chemical Engineering, McGill University, Montreal, QC, Canada H3A 2B2

Gary R. Marchand and Jian Wang

The Dow Chemical Company, 2301 North Brazosport Boulevard, Freeport, Texas 77541

Sheng Li and Richard A. Register

Department of Chemical Engineering, Princeton University, Princeton, New Jersey 08544

Received June 2, 2010; Revised Manuscript Received July 17, 2010

ABSTRACT: Several samples of a recently developed olefin multiblock copolymer were studied by means of rheology, differential scanning calorimetry (DSC) and small-angle X-ray scattering (SAXS). The synthesis involves a chain shuttling agent (CSA) that switches the growing chain between two catalysts, one that favors the incorporation of an α-olefin comonomer and one that suppresses incorporation. The data were used to determine the effect of octene comonomer content and CSA level on rheological behavior and the occurrence of mesophase separation transition (MST) in the melt. To distinguish between crystallization and MST, we made calorimetry scans and measured the density and rheological properties over a range of temperatures. Small angle X-ray scattering analysis of a sample that had undergone planar extensional flow revealed strong alignment of lamellar mesodomains, which maintained their alignment after annealing. This result confirmed the hypothesis based on rheological evidence that a lamellar mesophase is present in the melt at temperatures well above the melting point.

I. Introduction

Block copolymers have generally been made by means of living polymerization, most often using anionic techniques. By changing the monomer during the reaction, blocks can be assembled, and there is a large literature on di- and triblock, monodisperse, amorphous copolymers. If room temperature is intermediate between the glass temperatures of the two or three types of block, such systems are thermoplastic elastomers.[1,2] These systems undergo an order−disorder transition ODT in the melt to form nanoscale domains having several possible geometries.

I.A. Terminology. In much of the early literature on "classical" block copolymer systems, *i.e.*, monodisperse di- and triblock copolymers, the terms ODT and "microphase separation transition" were used interchangeably, and Leibler's theory of ODT[3] actually used only the term microphase separation transition. However, it was later recognized that large-amplitude composition fluctuations, not accounted for in the Leibler theory, can produce structure and influence dynamics at temperatures above that for ODT.[4] A block copolymer can still have a separated structure that lacks long-range order.[5] Because the structures formed at the phase separation transition in the system we studied are much larger (100 nm) than those observed in monodisperse di- and triblock systems (15−25 nm), we speak here of mesophase rather than microphase separation, and we focused on separation rather than ordered states in this study. We use MST to mean mesophase separation transition in this paper.

I.B. Earlier Olefin Block Copolymers. Living polymerizations have also been used to make olefin block polymers,[6] although these reactions are not useful for commercial production, because each catalyst particle makes only one molecule. Methods for making polypropylene stereoblock homopolymers have been reported based on a nonliving catalyst.[7] These are thermoplastic elastomers, but practical applications are limited by their high glass temperatures. Another approach is to use mixed catalysts, the products of which can react with each other. Dekmezian et al.[8] used two metallocene catalysts with a feed of ethylene and 1-butene. One catalyst yields primarily linear polyethylene and macromonomer, while the second favors incorporation of comonomer and macromonomer. The final mixture contains linear and branched, amorphous chains and semicrystalline "branch-block" chains.

I.C. Olefin Block Copolymers Made Using a Chain Shuttling Agent. In 2006, Arriola et al.[9] reported the development of a new class of products that they called "olefin block copolymers" (OBC). These OBCs are made in a continuous solution process that involves two catalysts and a "chain shuttling agent" (CSA) that switches the growing chain from one catalyst to the other at random intervals. The CSA is a metal alkyl complex such as diethylzinc (Et_2Zn). One catalyst suppresses the insertion of comonomer, while the other readily inserts comonomer. The final chain then consists of two types of block: "hard blocks" consisting essentially of ethylene homopolymer with very low levels of comonomer, and "soft blocks" of ethylene/higher α-olefin copolymer. The terms hard and soft are based on stiffness (or crystallinity) at room temperature. Figure 1 is a sketch showing the structure of these copolymers and the terminology used to describe them. Varying the relative catalyst concentrations controls the percentage of hard and soft blocks. Varying the

*Corresponding author.

Published on Web 07/28/2010

amount of CSA controls the block lengths, *i.e.*, the concentration ratio of Et_2Zn to ethylene, $[Zn]/[C_2H_4]$ controls the level of blockiness,[10] and varying the comonomer concentration controls the amount of comonomer incorporated into the soft blocks. Since this is a statistical process, the blocks produced have random distributions of both length and comonomer content. Increasing the CSA level leads to more and shorter blocks, and the limiting case of very high CSA is a random copolymer. Increasing CSA also narrows the molecular weight distribution, toward a limiting case of the Flory distribution with $M_w/M_n = 2.0$. The crystallization,[11,12] solid-state properties,[13] adhesion behavior,[14] comparison with random ethylene−octene copolymers,[15] phase behavior with ethylene−octene copolymers,[16] optical properties,[17] and general aspects[18] of OBCs have been reported previously.

Li Pi Shan and Hazlitt[10] proposed a quantitative measure of the degree of "blockiness" of an OBC, the block index BI, which is based on the difference between the comonomer distribution within an OBC chain and that for a statistically random copolymer. The average BI is positive for an OBC, zero for a random copolymer, and negative for an alternating polymer. The calculation of this index requires analytical temperature rising elution fractionation (ATREF) data, which were not available for our samples.

Another type of "coordinative chain transfer polymerization" (CCTP)[19] has been used to prepare diblock olefin polymers in continuous stirred tank reactors in series,[17,20] but our study dealt only with multiblock materials.

The study of semicrystalline block copolymers is complicated by the interference of crystallization with ODT and MST, and this issue has been explored in depth.[21−27] If the incompatibility between blocks is small, crystallization occurs from the homogeneous melt leading to a lamellar crystalline structure. But if the incompatibility is large, microdomains formed prior to crystallization can have a strong effect on subsequent crystallization. The OBCs of interest here are semicrystalline but have the additional complexity of being multiblock systems that are polydisperse in terms of both block molecular weight and the number of blocks per chain. In this regard they are similar to multiblock polyurethanes (PU),[28] but PU blocks are much shorter than those in OBCs, and their behavior is further complicated by hydrogen bonding.

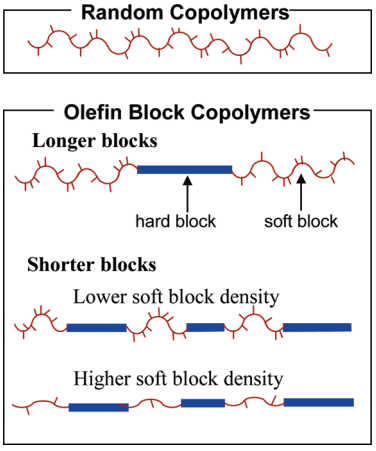

Figure 1. Sketch showing the structure of copolymers and the terminology used to describe them. The terms hard and soft are based on stiffness (or crystallinity) at room temperature.

II. Experimental Section

II.A. Materials Studied. We studied four ethylene−octene copolymers in which the ratio of chain shuttling agent to ethylene concentration and the total comonomer content were varied. Information about the molecular structure of the samples is provided in Table 1. Characterization methods are described elsewhere.[12] The concentration ratio of Et_2Zn to ethylene, $[Zn]/[C_2H_4]$ is a measure of the level of chain shuttling agent (CSA) used. Increasing the CSA concentration leads to a structure having more and shorter blocks.

There are two types of block in our OBC molecules: hard blocks incorporating very little octene and soft blocks with many hexyl branches. The terms hard and soft are based on stiffness at room temperature. Figure 2a is a sample "map" indicating the relative levels of chain shuttling agent and total octene content of our samples, and in Figure 2b, the ordinate is the average octene content of the soft blocks. There are two types of OBC in terms of octene content of the soft blocks: 17 and 27 mol %. R03 has the highest total octene content and R09 has the highest octene content of the soft blocks but less total octene since the total weight of soft blocks in R09 is much smaller than that in R03. Increasing the comonomer concentration during the synthesis increases the difference in octene content between the soft and hard blocks, and therefore increases the thermodynamic difference, tending to increase the temperature at which MST will occur in the melt. We were not able to establish a quantitative relationship between CSA level and average length of each type of block, because we do not know the number of chain transfers during synthesis. The actual block populations are affected by variables such as temperature and reactor design. All samples contained a combination of primary and secondary antioxidants that is commonly used for polyolefins.

II.B. Measurement Methods. We carried out differential scanning calorimetry (DSC) scans using a Perkin-Elmer Pyris 1 DSC from 50 to 180 and 180 to 50 °C for all samples. We used two rates: ±10 and ±0.45 °C/min. The former is the one generally used for DSC measurements, while the latter matches the temperature sweep rate used to measure the dynamic moduli as is described below.

We determined the density as a function of temperature between 30 and 220 °C by use of a Gnomix PVT instrument. The data followed eq 1 above 135 °C, and Table 3 gives values of the fitting constants, a and b.

$$\rho = \frac{1}{a + 10^{-3} bT} \tag{1}$$

Table 1. Molecular Structure of Samples[a]

	total blocks wt %		total octene content			octene content of soft blocks			octene content of hard blocks			
code	soft	hard	mol %	wt %	SCB[b] /10^3C	mol %	wt %	SCB[b] /10^3C	wt %	$10^3 \times [Zn]/[C_2H_4]$	M_w (kg/mol)	M_w/M_n
R01	73	27	11.5	34	58	17.9	47	90	~1	0.65	122	2.4
R03	74	26	16.6	44	83	26.5	59	133	~2	0.5	151	2.2
R09	52	48	13.9	39	70	27.5	60	138	~2	0.7	136	2.1
R17	75	25	12	35	60	17	45	85	~1	1.2	124	2.1

[a] Octene contents were determined by NMR, and molecular weights were determined by GPC.[12] [b] SCB/10^3C = the number of short chain (hexyl) branches per 1000 backbone carbon atoms.

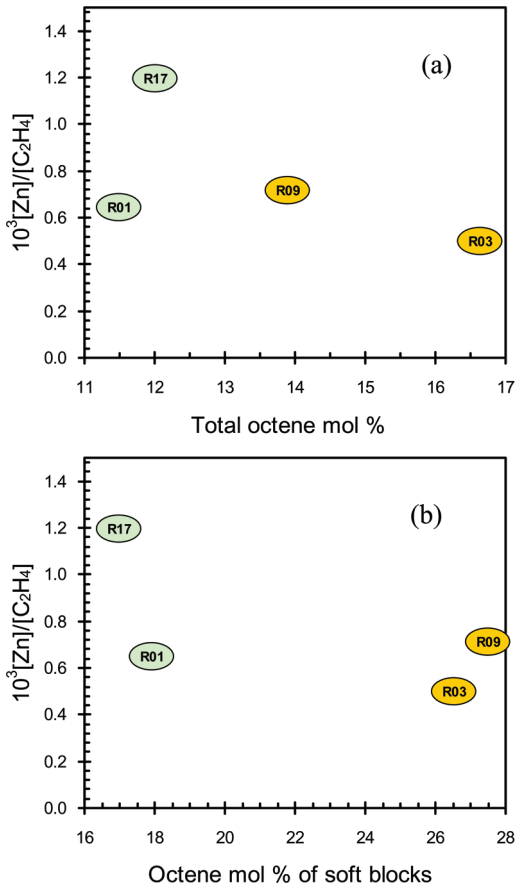

Figure 2. Maps of samples showing (a) CSA level and total octene content and (b) CSA level and octene content of soft blocks.

All rheological data were obtained using parallel disks with a diameter of 25 mm and a gap of 1 mm in rotational rheometers. Disk samples with a thickness of 1.1 mm were made of pellets by compression molding at 180 °C. Before and after molding, samples were stored in a vacuum oven at room temperature more than a week to minimize volatile matter, including unreacted monomers and oxygen. We performed time sweep of small-amplitude oscillatory shear (SAOS) tests in an SR5000 rheometer (Rheometric Scientific) to determine the experimental time limit for stability. All rheological measurements were performed within this limit, which was defined as the time at which the data changed by 3% from their initial values. Severe thermal degradation occurs at temperatures above 220 °C, so we chose 220 °C as our maximum working temperature.

Prior to frequency sweep tests of dynamic moduli, we performed strain sweep to define the experimental strain window for the linear viscoelasticity (LVE). By frequency sweep tests of dynamic moduli, we determined the plateau modulus, established the melting range, and obtained information on the melt structure. For frequencies in the range of $0.1 \leq \omega \leq 500$ rad/s we used a controlled strain instrument (ARES, Rheometric Scientific) while for lower frequencies ($0.01 \leq \omega \leq 40$ rad/s) a controlled-torque instrument (SR5000) was used. Data from the two instruments in the overlapping frequency range differed by less than 2%. In order to probe the terminal zone, long-time creep experiments were performed using the SR5000 after identifying the stress range for the linear creep compliance. To convert creep compliance data to storage and loss moduli, we used a nonlinear regularization algorithm (NLREG)[29] to obtain a retardation spectrum $L(\tau)$ from the creep compliance[30] using the generalized Voigt model, and $L(\tau)$ was then used to calculate the storage and loss compliances.[30] Finally, the storage and loss moduli were calculated[30] from the dynamic compliances.

Temperature sweep tests of dynamic moduli were performed using the ARES rheometer at a frequency of 1 rad/s and a strain amplitude of 1% to identify melting and crystallization zones. A sample was loaded at 220 °C, cooled to 105 °C, and then reheated to 130 °C while rheological data were obtained at intervals of 0.5 °C. The sample was soaked at each temperature for 50 s, and we found no difference between data obtained with soaking times of 50 and 120 s. The overall heating/cooling rates were ±0.45 °C/min. We chose this low rate to obtain data comparable to those from isothermal measurements. Thermal expansion of the upper and lower disks was taken into account for the resulting moduli values but not the thermal expansion and shrink of the sample.

Another type of temperature sweep test was carried out to determine the mesophase separation transition temperature T_{MST}. A sample was loaded at 220 °C, cooled to 150 °C, left at this temperature for 1 h with no measurement, and then finally reheated to 220 at 0.1 °C/min with measurements at intervals of 1 °C with a soaking time of 1 min at each temperature. Thermal expansion of the upper and lower disks was taken into account, and the thermal expansion and shrink of the sample was considered during analysis (eq 9).

Small-angle X-ray scattering (SAXS) patterns were acquired at the DuPont−Northwestern−Dow Collaborative Access Team (DND-CAT) beamline (5ID-D) at the Advanced Photon Source, Argonne National Laboratory. The X-ray energy was set at 10 keV (λ = 0.12398 nm). SAXS data were collected on a MAR USA CCD camera at a sample-to-detector distance of 8 m.

III. Melting and Crystallization Temperatures

For crystallizable block copolymers the study of MST is problematic when the MST temperature is close to the crystallization temperature. It was thus important to distinguish between these two types of transition. While crystallization has a larger effect on density than MST, *PVT* data have insufficient precision to pinpoint crystallization temperatures, and we carried out differential scanning calorimetry (DSC) scans at ±10 °C/min from 50 to 180 °C and 180 to 50 °C, and the results are shown in Figure 3. Peak temperatures ($T_{m,peak}$ and $T_{c,peak}$) are defined as the maximum and minimum points of each heating and cooling peak as generally reported. These transition temperatures are given in Table 2. We determined the crystallinity by dividing ΔH_m (the peak area of a melting curve with time) by the theoretical heat of melting, ΔH_m = 290 J/g[31] for 100% crystalline polyethylene. Crystallinities at 50 °C are given in Table 2, based on both the entire mass and the hard block mass. The latter figure is a rough estimate based on the assumption that all the crystallinity is in the hard blocks. The resulting hard-block crystallinities are 51% for R09 and 76% for R01. Thus, R01, which contains the least comonomer, has the highest crystallinity as we can expect.

Figure 4b shows DSC scans from 50 to 180 °C and 180 to 50 °C at ±0.45 °C/min. It has been reported[32,33] that DSC peaks appear at ODT for block copolymers, but the density data shown in Figure 4a reveal a large change in density over the same range of temperatures, so we are confident that our DSC peaks correspond to melting and crystallization. There is no abrupt decrease in density above 129 °C. As expected, the width of the peak at ±0.45 °C/min is narrower than that at ±10 °C/min. Completion of melting or crystallization occurs earlier at a rate of ±0.45 °C/min than at ±10 °C/min, although the rate dependence of melting is much weaker than that of solidification. We define $T_{m,com}$ and $T_{c,com}$ as the temperatures at the end of the peak of the heating and cooling curves, respectively. The starting point of the peak of the heating and cooling curves is not clear, so $T_{m,start}$ and $T_{c,start}$ are not obtained from DSC curves.

Table 2. Transition Temperatures and Crystallinity

	transition temperatures from DSC at ±10 °C/min (°C)		transition temperatures at ±0.45 °C/min from DSC expect for $T_{c,start}$ and G' (T) (°C)			crystallinity at 50 °C (%)	
code	$T_{m,peak}$	$T_{c,peak}$	$T_{m,com}$	$T_{c,start}$	$T_{c,com}$	based on total material mass	normalized to hard block mass
R01	123.8	102.0	126	116	109	20.4	76
R03	117.4	98.0	120	109	102	16.2	62
R09	118.4	102.3	120	111	103	24.4	51
R17	123.1	98.3	125	114	107	18.0	72

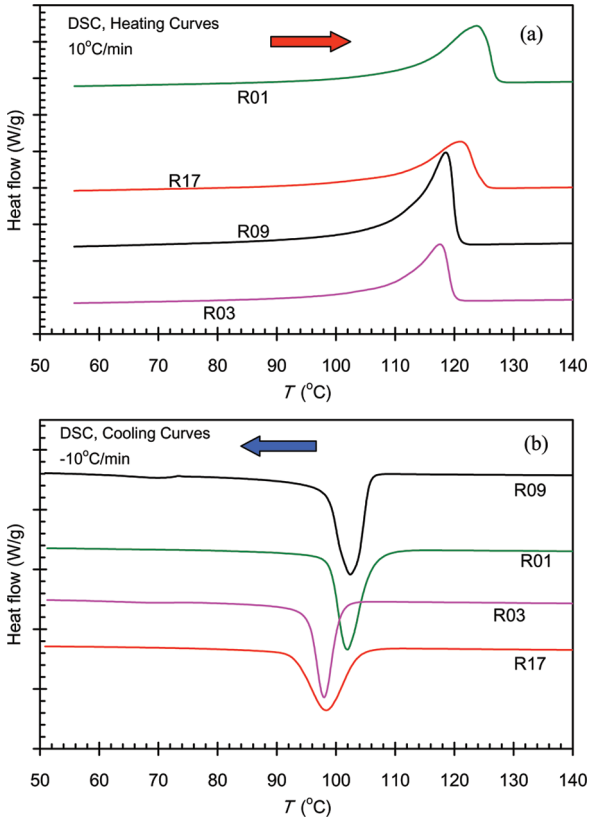

Figure 3. DSC scans at ±10 °C/min for all samples.

Figure 4c shows results for temperature sweep tests of storage modulus for R01. We define $T_{m,com}$ as the temperature where the large decrease in G' ends, *i.e.*, where melting is completed and G' starts decreasing smoothly following a straight line on the semilog plot. We define $T_{c,com}$ as the temperature where the large increase in G' ends, *i.e.*, where crystallization is completed and G' starts increasing smoothly following a straight line on the semilog plot. Unlike the DSC scans, G' shows more clearly the starting point of the peak of the cooling curve, so we can obtain $T_{c,start}$. However, the starting point of the heating curve was not clear like the DSC scans. We see similarities with the DSC scan at the same cooling and heating rates (±0.45 °C/min) as indicated by dash-dot lines. The peak points, $T_{m,peak}$ and $T_{c,peak}$ from DSC scans appear to correspond to the inflection points of G', but more G' data points would be needed to confirm this correspondence. Table 2 lists the transition temperatures.

All the OBCs in this study show a single large change of moduli in each direction of cooling or heating, and no sample shows a sudden change above 129 °C. These rheological data provide clear evidence of crystallization around 110 °C and complete melting below 130 °C which is well below the temperatures at which we observed evidence of mesophase structure in the melt. We are thus confident that our reports of mesophase formation involve temperatures well above the melting zone.

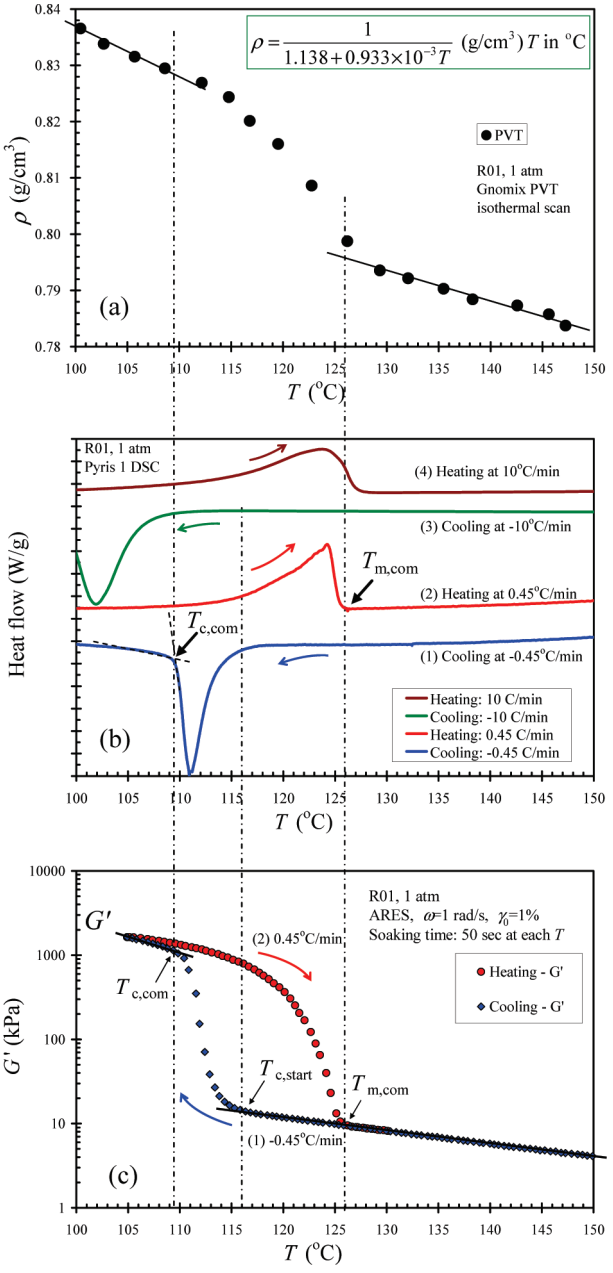

Figure 4. Comparison between three types of temperature sweep test for R01: (a) density; (b) DSC scans with cooling and then heating at ±10 and ±0.45 °C/min; (c) storage and loss moduli with cooling and then heating at ±0.45 °C/min.

IV. Rheological Behavior

We measured the storage and loss moduli at four or five temperatures above the melting temperature. To prepare master curves, we took the vertical shift factor to be unity, and the horizontal shift factors were based on a reference temperature of T_0 = 220 °C. As has been observed in earlier studies of block

Table 3. Rheological Parameters and Density

code	G_C (kPa)*	G_N^0 kPa (eq 3)*	M_e kg/mol (eqs 3 and 6)*	M_b g/mol (eq 5)	G_N^0 kPa (eq 4)	M_e kg/mol (eqs 4 and 6)	a_T*	E_a kJ/mol	parameters of eq 1 (130 < T < 220 °C) a (cm^3/g)	b (cm^3/g°C)	η_0 (kPa s) 135 °C	220 °C	parameters of eq 7 C_1	C_2 (°C)	ω'_C (rad/s)
R01	93.9	742	3.60	18.83	882	3.03	7.1	38.8	1.138	0.933	33.9	3.9	−1.54	219.6	6
R03	68.2	505	5.26	20.97	606	4.38	8.1	41.1	1.135	1.032	682.2	12.1	−1.75	167.0	60
R09	77.2	551	4.86	19.84	735	3.70	8.0	40.3	1.152	0.749	1365.0	34.2	−1.32	158.0	90
R17	115.6	820	3.27	19.04	849	3.21	7.0	37.9	1.132	0.867	39.4	5.1	−3.32	414.1	5

*At 135 °C.

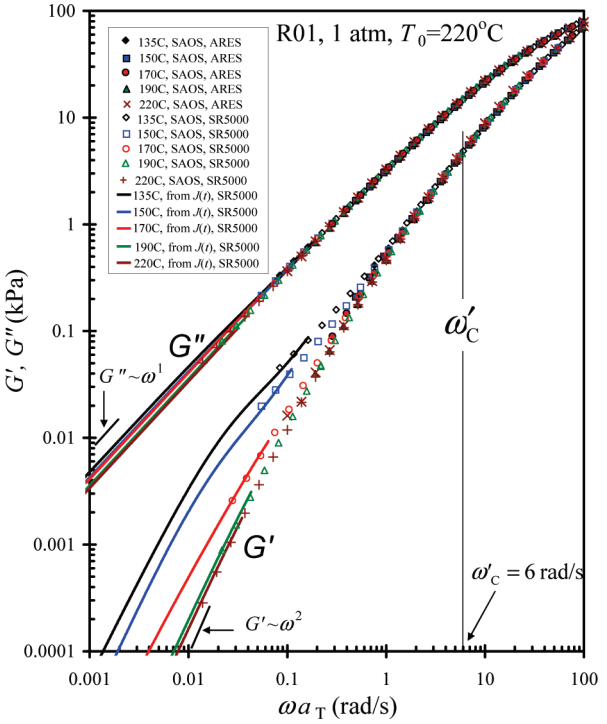

Figure 5. Reduced storage and loss moduli from SAOS for R01 along with behavior extended to the terminal zone by use of creep measurements. The vertical shift factor is taken to be unity, and the horizontal shift factor is based on behavior at higher frequencies.

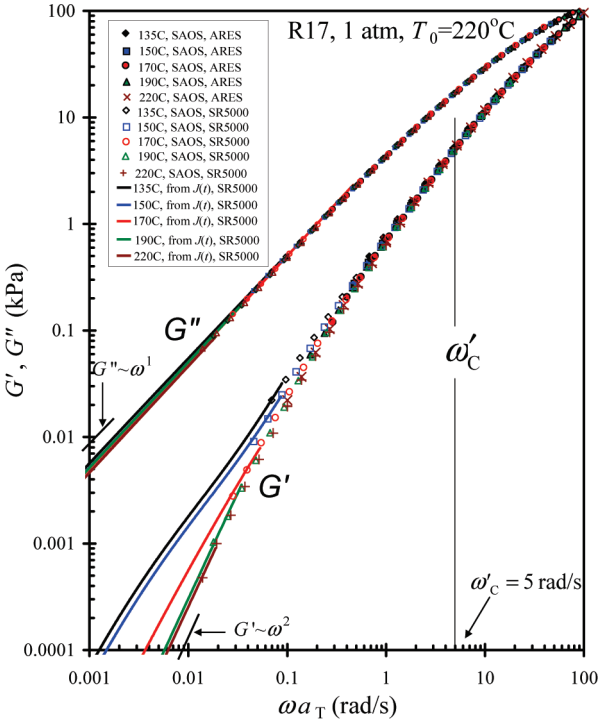

Figure 6. Reduced storage and loss moduli from SAOS for R17 along with behavior extended to the terminal zone by use of creep measurements. The vertical shift factor is taken to be unity, and the horizontal shift factor is based on behavior at higher frequencies.

copolymers,[34] time−temperature superposition failed either at temperatures significantly above the melting point but below 220 °C (R01 and R17) or at all temperatures except at high frequencies (R03 and R09). Horizontal shifting was based on data at temperatures where time−temperature superposition (TTS) was valid and the system was believed to be homogeneous or on data at high frequencies. The failure of TTS is known to be a sign of microphase separation in monodisperse di and triblock systems, and its implications for our samples is discussed in detail below. Figures 5−8 show master curves of storage and loss moduli of the four samples studied, and Figure 9 shows the magnitude of the complex viscosity of sample R09.

The Arrhenius model (eq 2) was found to describe the temperature dependence of the horizontal shift factor $a_T(T)$ for all of our samples.

$$\ln[a_T(T)] = \frac{E_a}{R}\left(\frac{1}{T}-\frac{1}{T_0}\right) \quad (2)$$

where R is the gas constant and E_a is the activation energy for flow. This expression does not apply to the zero-shear viscosity because of the failure of TTS at low frequencies. Values of E_a are shown in Table 3. Figure 10a shows that octene level increases E_a, and this trend is consistent with the fact that any side group attached to a polyethylene backbone increases the temperature sensitivity of its rheological properties. Figure 10b shows that CSA level decreases E_a for samples with similar octene content. In other words, E_a increases with block length.

Because storage and loss moduli of samples with broad molecular weight distributions do not have the clearly defined features that make it possible to infer the rubbery plateau modulus G_N^0 directly from rheological data, indirect methods are used to estimate G_N^0 for such materials. These methods have been described by Dealy and Larson,[35] and some of these are based on correlations and models.[35] Liu et al.[36] concluded that in the case of polydisperse, semicrystalline polyolefins, only the method based on the crossover modulus $G_C = G'(\omega) = G''(\omega)$ is useful. The relationship proposed by Wu[37] is:

$$\log\left(\frac{G_N^0}{G_C}\right) = 0.38 + \frac{2.63\log(M_w/M_n)}{1+2.45\log(M_w/M_n)} \quad (3)$$

This correlation involves only a single parameter, M_w/M_n, to describe polydispersity, and Liu et al.[36] comment that the values obtained should be used only for qualitative comparisons. They found that the use of G_C yielded values of G_N^0 that were significantly lower than those calculated using the more reliable integration method.

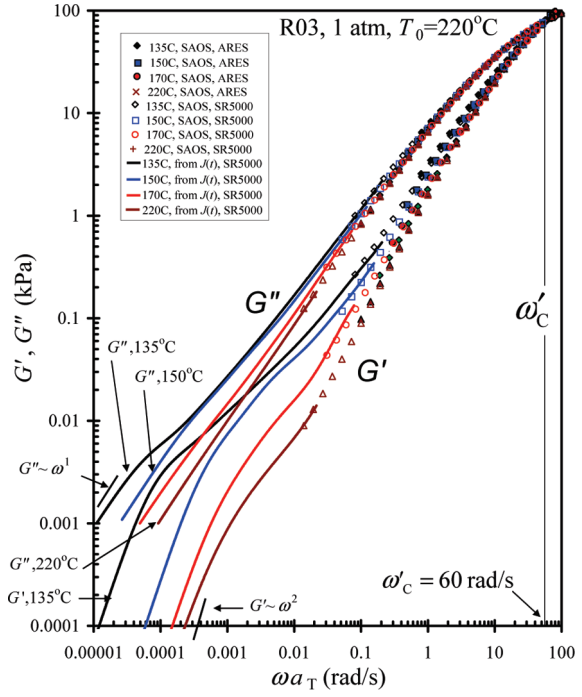

Figure 7. Reduced storage and loss moduli from SAOS for R03 along with behavior extended to the terminal zone by use of creep measurements. The vertical shift factor is taken to be unity, and the horizontal shift factor is based on behavior at higher frequencies. To avoid crowding, data at 190 °C are omitted.

However, the materials that we studied have relatively narrow molecular weight distributions that are described quite well by the Flory, most-probable distribution. While there will be uncertainty in comparing values obtained using eq 3 among polymers of different types, we are confident that the values reported here provide a reliable basis for comparing our samples with each other.

The resulting G_N^0 values are shown in Table 3. García-Franco et al.[38] showed that G_N^0 decreases with octene comonomer content, and Liu et al.[36] observed the same trend for several semicrystalline polymers. We also saw differences among samples having varying octene contents.

Fetters et al.[39] reported an approximate correlation between the plateau modulus and the average molecular weight per backbone bond M_b for a number of olefin copolymers, which is shown as eq 4.

$$G_N^0 = 24820 M_b^{-3.49}\ (\text{MPa}) \quad (14 \le M_b \le 28\ \text{g/mol}) \qquad (4)$$

where G_N^0 values were obtained by integrating $G''(\omega)$ or from the maximum value of $G''(\omega)$.[40] The parameter M_b depends on comonomer content and size but not on block structure. For ethylene−octene copolymers, M_b is related to m_O, the octene mole fraction, as follows:

$$M_b = 42 m_O + 14\ (\text{g/mol}) \qquad (5)$$

Values of G_N^0 and M_b for our samples are given in Table 3 and are plotted in Figure 11 along with values given by Fetters et al.[39] The OBC polymers follow the same trend as the copolymers considered by those authors. No theoretical basis has been suggested for this approximate correlation.

Table 3 indicates that CSA level has little effect on G_N^0 of samples R01 and R17 which have about the same soft-block octene content. In other words, block length has little effect on G_N^0.

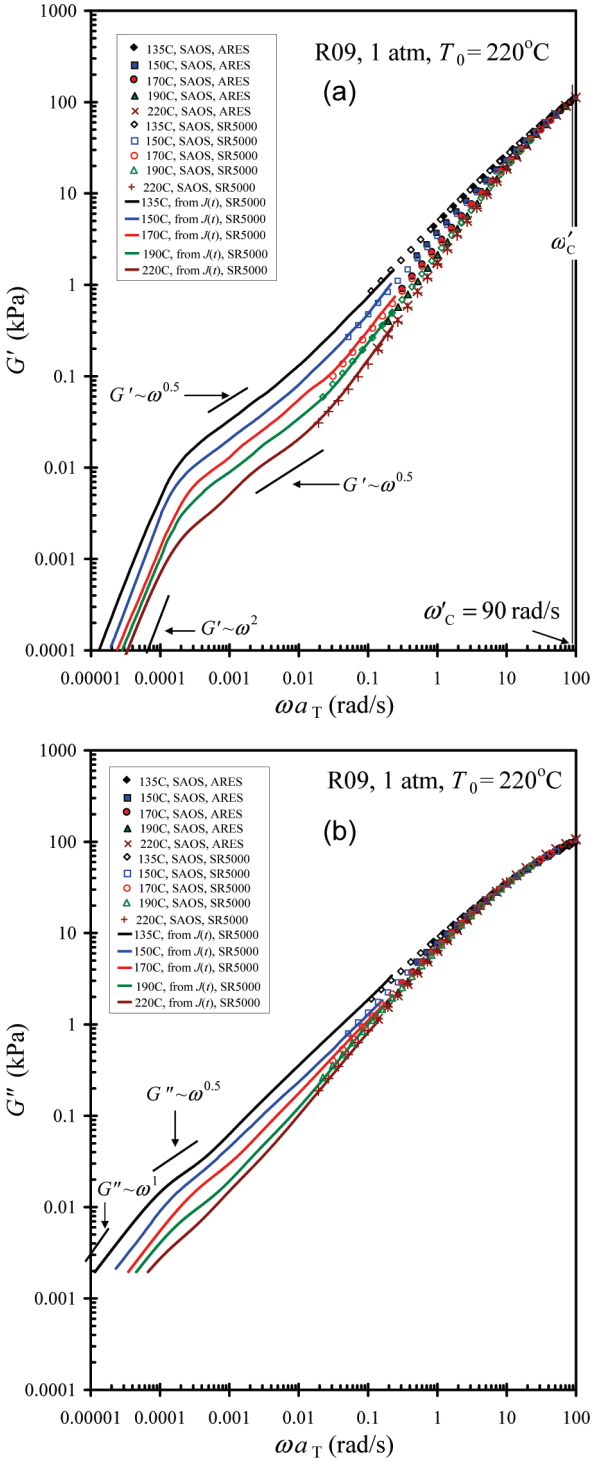

Figure 8. (a) Reduced storage modulus for R09 and (b) reduced loss modulus for R09. The vertical shift factor is taken to be unity, and the horizontal shift factor is based on behavior at higher frequencies.

Two definitions of the molecular weight between entanglements M_e, differing by a factor of 4/5, are in current use,[35] and we used the one originally proposed by Ferry[30] which is shown as eq 6.

$$M_e \equiv \frac{\rho RT}{G_N^0} \qquad (6)$$

The molecular weight between entanglements increases with chain stiffness and is an important parameter in tube models of

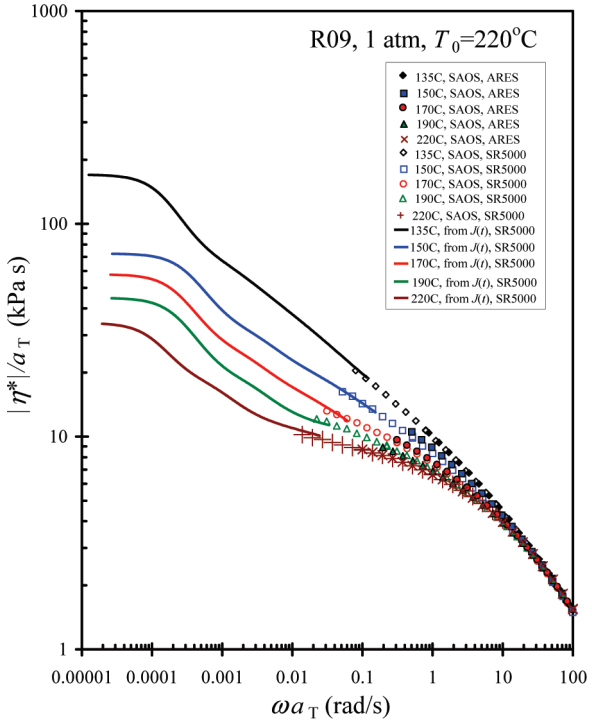

Figure 9. Reduced magnitude of complex viscosity for R09. The vertical shift factor is taken to be unity, and the horizontal shift factor is based on behavior at higher frequencies.

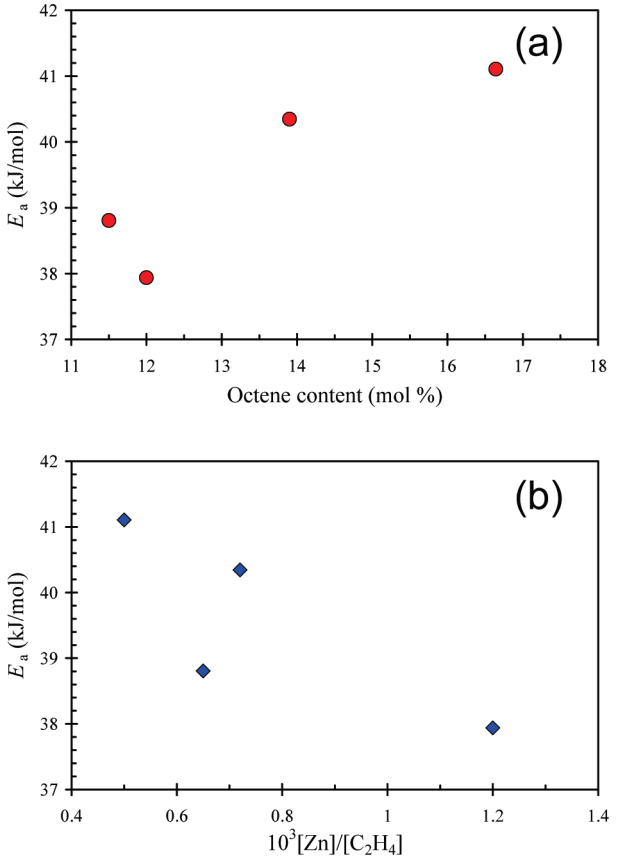

Figure 10. Activation energy for flow obtained from horizontal shift factors by use of eq 2: (a) effect of total octene content; (b) effect of CSA level.

viscoelasticity. This quantity is independent of average molecular weights and molecular weight distribution for well-entangled,

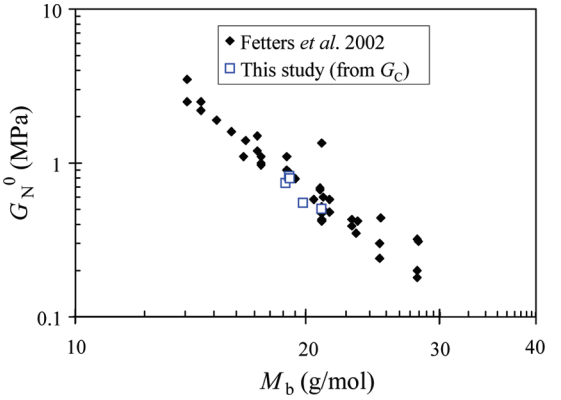

Figure 11. Plateau modulus versus average molecular weight per backbone bond. Open symbols are our data, and filled symbols are as reported by Fetters et al.[39]

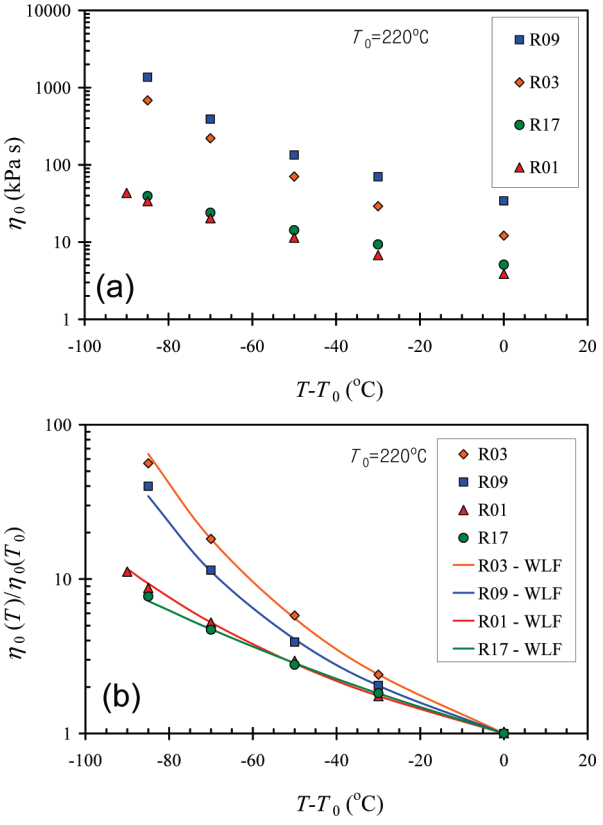

Figure 12. Zero-shear viscosity obtained from the long time linear creep compliance or SAOS. Key: (a) zero-shear viscosity versus temperature; (b) zero-shear viscosity ratio versus temperature giving data and WLF model prediction.

linear polymers, but it depends on molecular structure. In ethylene/α-olefin copolymers, increasing the comonomer content decreases G_N^0 thus increasing M_e. This effect has been noted for ethylene/butene and ethylene/octene copolymers,[41] and our materials follow the trend. It is also known that propylene copolymers have much lower values of G_N^0 than ethylene copolymers.

V. Mesophase Separation

V.A. Rheological Evidence. As shown in Figures 5−8, creep measurements made it possible to reach a terminal zone, and zero-shear viscosities were determined. The values of zero-shear viscosity η_0 are plotted as a function of temperature in Figure 12a, and are given at two temperatures

in Table 3. Except for samples R01 and R17 at the highest two temperatures, η_0 is affected by large composition fluctuations and/or mesophase separation and thus is not related to weight-average molecular weight as it is for linear polymer. Kossuth et al.[42] stated that at sufficiently low frequencies, even at temperatures well below T_{MST} block copolymers should exhibit terminal behavior with the classical slopes of two and one for log G' and log G'' versus log ω respectively. Terminal behavior in block copolymers at temperatures below T_{MST} has rarely been reported because of the extremely low frequencies required, but it was observed by Sebastian et al.[43] for sphere-forming block copolymers. They suggested that in cubic systems of block copolymers, terminal behavior corresponds to defect mediated creep (as in metals, for example) without which a material would have a nonzero modulus at infinite time. Lamellar polymers have defect structure as well, so perhaps that is what we are seeing at the lowest rates. However, there are two reasons why the situation may not be entirely analogous: (1) Lamellae do not form a 3D structure (like the bcc lattice of spheres). So if one were to measure a perfectly aligned lamellar structure, with the shear gradient parallel to the lamellar normal, it should have a zero modulus at infinite time because the layers can slip or slide relative to each other without changing the spacing or requiring defects. That is why lamellar specimens do not typically show a "lattice modulus" region as spheres do.[43] (2) Lamellae have a strong propensity to align in flow unlike spheres, which remain polygrain always.

The total strain applied in the creep experiments varied from 2.5 (at 135 °C) to 5.7 (at 220 °C) for R09, and the stress was between 1.5 and 3 Pa. This much deformation and stress in a unidirectional shear is well lower than those that can induce strong alignments,[44] but it can still produce a modest anisotropy,[44] which may not appear during SAOS tests. It should be noted that once a sample is aligned during a creep test, this sample will be different from a fresh sample. Thus, the zero-shear viscosity obtained from SAOS, if ever possible, will be lower than that from creep compliance. Another consecutive rheological measurement may not be used to confirm the alignment formation due to the creep, for example performing another creep test after the first one. We have to wait until the melt is out of a disturbed state, but there will be severe thermal degradation while we are waiting for the full relaxation because R03 and R09 have very long relaxation times and will relax very slowly after stopping the creep.

Curiously, the WLF equation,[45] shown as eq 7, provided a good fit to the variation of η_0 with temperature (Figure 12b), and the parameter values are given in Table 3. Since these melts are far above their glass points, free volume is not relevant, and the values of C_1 and C_2 that are listed in the table have no known physical significance.

$$\log\left[\frac{\eta_0(T)}{\eta_0(T_0)}\right] = \frac{C_1(T-T_0)}{C_2+(T-T_0)} \qquad (7)$$

Rheological behavior has been found to be a useful tool for the study of MST in monodisperse di- and triblock systems,[34,46,47] and we found this to be the case for our samples. At temperatures below the T_{MST} but above the glass temperature of either block, the material is molten, but its linear viscoelastic behavior at low frequencies deviates from that of a homogeneous system. In particular, time−temperature superposition (TTS) fails, and the curve of storage modulus versus reduced frequency takes on a distinctive form depending on the temperature and the morphology of the phase, as shown in Figure 13, a representation proposed by Kossuth et al.[42] We used high frequency portions to obtain the horizontal shift factors and master curves.

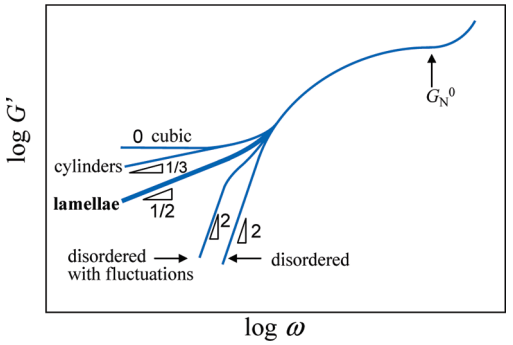

Figure 13. Sketch from Kossuth et al.[42] showing storage modulus versus frequency behavior for several types of block copolymer system at a temperature below MST. The behavior of our samples shows the types of behavior labeled "disordered", "disordered with fluctuations", and "lamellae".

Figures 5 and 6 are master curves for R01 and R17, which have similar octene levels but different CSA levels. While the G'' data appear to superpose well, G' clearly reveals failure of TTS. Since G' makes a small contribution to $|\eta^*|$, some degree of TTS failure can be seen in $|\eta^*|/a_T$. Figures 7 and 8 are master plots for R03 and R09, which have similar CSA levels. These samples have higher octene content than R01 and R17, and we see that both G' and G'' obtained at various temperatures show strong TTS failure. This implies that R03 and R09 always exhibit TTS failure within the experimental temperature range, *i.e.*, MST occurs in these samples even at very high temperatures, which well exceed the realistic experimental range, and that phase separation is much more severe than that in the samples that have lower octene content. Since G' and G'' values of R09 fall very close together, they were plotted separately. Bates et al.,[34,48] found that each of the olefin diblock copolymers they studied exhibited failure of TTS at a characteristic value of reduced frequency, which they called ω'_c. We observed the same behavior, and the resulting values are indicated in Figures 5−8 and tabulated in Table 3.

The first, weak departure from time−temperature superposition as temperature is decreased results in a shallow shoulder and a delayed but accessible terminal zone. As indicated in Figure 13, this behavior of the disordered phase above MST has been attributed to large-amplitude concentration fluctuations,[48,49] which were predicted by a theory of Fredrickson and Helfand.[50]

As the temperature is reduced below that at which failure of TTS first occurs, earlier studies of block copolymers have reported a large change in the shape of the $G'(\omega)$ curve over a very narrow temperature range. As indicated in Figure 13, at MST the data jump from a weak shoulder due to composition fluctuations to a more prominent one characterized by a slope that depends on the structure formed and is much less than the terminal slope of two. Such a dependency has been predicted for lamellar structures in different ways by Kawasaki and Onuki[51] and by Rubinstein and Obukhov.[5] Figures 7 and 8 show that data for samples R03 and R09 move onto curves with slopes of about 0.5 as temperature decreases, suggesting that these samples undergo a MST to a lamellar structure.

However, we see in Figure 7 that R03 shows weaker evidence of mesodomain structure than R09 and has the 0.5 slope only at 135 °C, suggesting that R03 has a less well-defined structure than R09. The asymmetric composition of

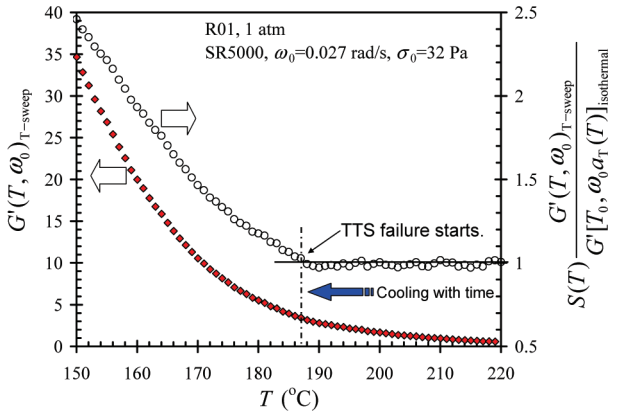

Figure 14. Determination of temperature where TTS first fails by means of temperature sweep of SAOS data. Temperature sweep was performed from 150 to 220 °C at an average rate of 0.1 °C/min with 60 s soaking time at each temperature.

R03 (26/74 hard/soft by weight) may contribute to this behavior, as this asymmetry raises the value of χN required for domain formation, where χ is the Flory interaction parameter, and N the average degree of polymerization of the blocks; it can also alter the type of mesophase formed (e.g., cylinders vs lamellae).[52] Samples R01 and R17, which contain much less octene than R03 and R09, do not exhibit $G'(\omega)$, $G''(\omega) \sim \omega^{0.5}$ at any temperature, but we do see an effect of CSA level.

Some aspects of the behavior we observed were reported by Bates et al.,[34,46] who studied several hydrogenated diblock copolymers of isoprene and 1,2 butadiene, *i.e.*, poly(ethyelenepropylene)−poly(ethylethylene), which can be thought of as olefin copolymers. They used both small-angle neutron scattering and rheology and observed a T_{MST} that depended on molecular weight, below which there was clear evidence of lamellar structure. Below T_{MST}, time−temperature superposition failed below a certain reduced frequency, ω'_C, with the storage modulus reaching a 0.5-power dependence on frequency at the lowest frequencies accessible. A distinctive feature of their master plots of $G'(\omega)$ was a major jump from a weak shoulder due to composition fluctuations onto a curve having a segment with slope 0.5. However, we did not observe such a jump, and for our materials the shift from one type of curve to the other occurred gradually over a range of temperatures. To investigate this behavior in more detail, we performed temperature sweeps at a fixed frequency.

In the study of diblock copolymers, plots of $G'(T)$ at a fixed frequency have revealed that G' drops sharply by a factor of at least three around T_{MST}.[34,46] To obtain data for such a plot, it is important to select the right frequency. The LVE data at this frequency must show failure of TTS, and this suggests the use of a low frequency. But one also needs to minimize time at each temperature and thus thermal degradation. We chose a frequency of $\omega_0 = 0.027$ rad/s for R01. Superheating is less likely than supercooling, because destroying structure is faster than creating structure, so we used a temperature rising sweep to determine the temperature at which TTS starts to fail. To eliminate the previous thermal history we loaded the sample at 220 °C. After we cool the sample down to 150 °C, we swept from 150 to 220 °C at an average rate of 0.1 °C/min with 60 s soaking time at each temperature. Figure 14 shows the result for sample R01 (solid diamonds). There are in fact three contributions to the effect of temperature, and we are only interested in one of them, and we normalized the data to show only departures

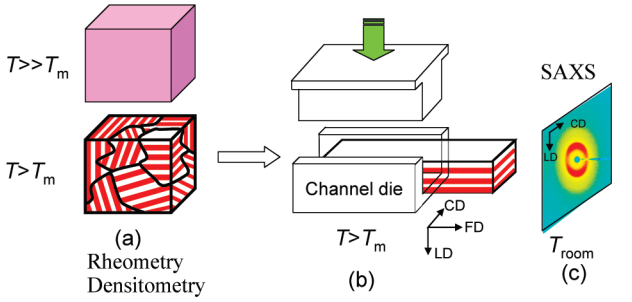

Figure 15. Schematic of separation structure. Key: (a) rheometry and densitometry were performed with multigrain structure of unaligned lamellar at low temperature ($T > T_m$) and homogeneous structure at high temperature ($T \gg T_m$), (b) flow in channel at low temperature tends to align the lamellar normals along the loading direction (LD), and (c) SAXS pattern is shown at room temperature.

from TTS. First, there is the normal effect of temperature described by the shift factor. To eliminate this effect we normalized the measured sweep data by dividing by the modulus calculated using the horizontal shift factor determined from the portion of the data that did obey TTS as shown in Figure 5.

$$\frac{G'(T,\omega_0)_{T-sweep}}{G'[T_0,\omega_0 a_T(T)]_{isothermal}} \tag{8}$$

A second temperature effect results from starving the gap due to the change in density of a sample as it expands and shrinks during a temperature sweep. We normalized to eliminate this effect by use of the following factor:

$$S(T) \equiv \frac{G'(T,\omega_0)_{isothermal}}{G'(T,\omega_0)_{T-sweep}} \tag{9}$$

where the numerator is G' measured while the gap was filled. Since there are only four data points for the numerator within the test range, $S(T)$ was fitted to a quadratic equation for the next step. Finally, we plot the following function, which is equal to unity if the data obey TTS:

$$S(T)\,\frac{G'(T,\omega_0)_{T-sweep}}{G'[T_0,\omega_0 a_T(T)]_{isothermal}} \quad \text{versus} \quad T \tag{10}$$

For samples other than R01, such a plot will not reveal interesting behavior. Since R03 and R09 do not show TTS within the range of working temperature, we do not expect a constant value of unity to appear. Because R17 shows a small degree of TTS failure, we can expect only a small deviation from unity. The normalized modulus (eq 10) is shown in Figure 14 (open circles). There is no sudden drop such as that observed for monodisperse diblocks[46] at a well-defined MST temperature, but we do see a growing departure from TTS (higher than one) as the temperature decreases below 187 °C, which is still well above the melting point. We believe that the absence of a sharp transition from composition fluctuations to MST is due to the polydispersity of OBCs in terms of both molecular weight and molecular structure. For this reason, it is not possible to assign a specific temperature to MST, but only a temperature where TTS starts to fail, which is 187 °C for sample R01.

V.B. Flow-Induced Alignment. Since the measurements described above (rheometry and densitometry) do not involve significant flow or deformation, we do not expect to see any strong alignment.[44] Figure 15(a) is a schematic of the

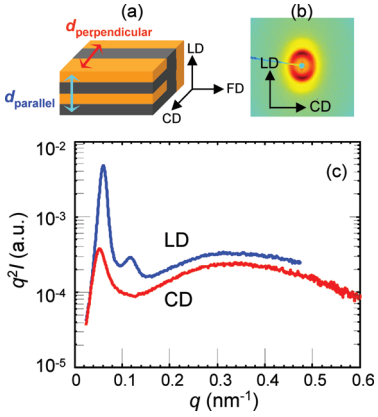

Figure 16. Data from SAXS at room temperature for R09 after extension at 160 °C: (a) schematic of lamellar orientation, with channel die axes indicated, (b) two-dimensional SAXS pattern with the X-ray beam aligned along FD, and (c) one-dimensional SAXS intensities versus the scattering vector q along LD and CD.

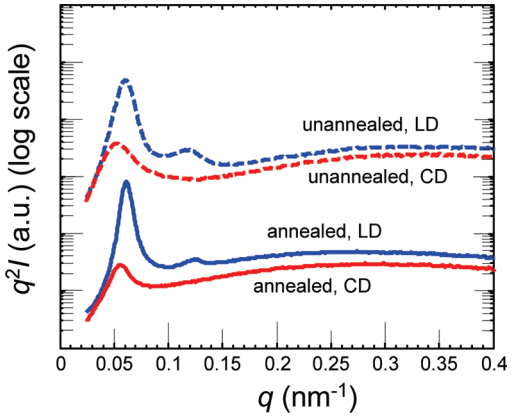

Figure 17. Comparison of room-temperature one-dimensional SAXS patterns for R09 (a) crystallized 20 min after extension (dashed curves) and (b) crystallized after annealing in the melt at 160 °C for 10 h.

multigrain structure of unaligned lamellae at relatively low temperature ($T > T_m$) and of a truly dissolved structure at very high temperature ($T \gg T_m$). However, both large-strain shear[44,53] and extensional[54] flows have been shown to strongly align phase-separated lamellar block copolymers. To examine this possibility in our materials, we studied the SAXS patterns of specimens of R09 that were flow-aligned in the melt. Sample R09, which shows the largest thermodynamic difference between hard and soft blocks, was subjected to planar extensional flow in the lubricated channel die [Figure 15(b)] described by Lee et al.[54] and by Li et al.[55] at 160 °C, which is well above the melting point but below the temperature at which the melt becomes thermorheologically homogeneous. The low-viscosity PDMS used for lubrication,[56] and the deformation is thus very close to planar extension (no shear). This flow field tends to align the lamellae normal along the loading direction (LD). The channel flow is generated by squeezing flow using a hydraulic press, and the compression ratio, *i.e.*, the total strain, is 7.5. Unfortunately, the X-ray contrast in the melt between the hard and soft blocks, both of which are ethylene−octene copolymers, is too small to reveal peaks even if present. However, if the oriented melt structure is retained following quiescent crystallization, room-temperature SAXS patterns will reflect the orientation imposed on the melt. Conversely, if crystallization "breaks out" from the regions occupied by the crystallizable segments in the melt, then an isotropic SAXS pattern bearing little relation to the melt structure will be observed.[23,57]

The flow-aligned melt is held at 160 °C for 20 min, then quenched in a dry ice/2-propanol bath at −78 °C. Figures 15c and 16 shows the room-temperature 2D SAXS pattern for flow-aligned R09, taken with the X-ray beam parallel to the flow direction (FD). The scattering pattern shows orientation anisotropy, with the highest scattering intensity concentrated along LD, consistent with R09 having an ordered morphology where the domains are predominantly aligned along FD, as depicted schematically in Figure 16a. Figure 16c shows the corresponding 1D intensity profiles, taken along LD and CD (constraint direction). Each intensity profile was q^2-corrected to account for the appropriate form factor scattering, where $q = (4\pi/\lambda) \sin \theta$, λ is the radiation wavelength, and 2θ is the scattering angle. There are two notable features in Figure 16c: a broad peak near $q \approx 0.3$ nm^{-1}, resulting from the stacking of polyethylene crystallites; and peaks of the LD profile at smaller q (< 0.15 nm^{-1}) which appear in a q ratio of 1:2,[58] reflecting a lamellar domain structure preserved from the melt. The characteristic interlamellar domain spacing, d, can be calculated from the position of the primary SAXS peak, q^*, via the following equation:

$$d = \frac{2\pi}{q^*} \tag{11}$$

Thus, we can estimate the repeat distance of the parallel-type lamellar domains (lamellar normal parallel to LD) as $d_{parallel} = 2\pi/0.0605 = 104$ nm.

To improve the order of the lamellar mesodomains, we annealed the channel-die-processed specimen in the melt, outside of the channel die and unconstrained, in a vacuum oven at 160 °C for 10 h, and then recrystallized it by removing it into ambient air. The FD-view SAXS profiles for the melt-annealed specimen are qualitatively similar to that from the unannealed sample but show better definition of all features, as shown in Figure 17: sharper SAXS reflections, a better resolved second-order SAXS peak along LD, and an increase in the difference in SAXS primary peak intensity along LD vs CD. Annealing in the melt at 160 °C evidently allows the mesodomain structure to perfect itself prior to crystallization, further confirming the phase-separated state of R09 at 160 °C. Li et al.[55] used SAXS to show that a material with a mesostructure similar to that of R09 is readily aligned by extensional flow and that annealing in the melt prior to crystallization improves long-range order of the lamellar mesostructure. This is in accord with the results shown in Figures 16 and 17.

Examination of Figure 16b reveals that although the highest scattering intensities are concentrated along LD, there is nonzero SAXS intensity along CD. This indicates that the alignment in the specimen is not perfect: while the predominant orientation of the lamellar normals are along LD (parallel-type lamellae, blue curves in Figures 16c and 17), there exists a minor population of lamellae whose normals are along CD (perpendicular-type lamellae, red curves). Upon annealing, the position of the peak associated with the parallel-type lamellae scarcely changes (from 0.0605 to 0.0613 nm^{-1}, or $d_{parallel} = 104$ to 102 nm), while the peak associated with the perpendicular-type lamellae shifts to higher q (0.0527 to 0.0565 nm^{-1}, or $d_{perpendicular} = 119$ to 111 nm), suggesting that the differently oriented lamellae approach (but do not reach) a common spacing after 10 h of annealing. The large long period due to the mesodomain structure is discussed in detail by Li et al.[55]

VI. Conclusions

The molecular weight between entanglements, M_e, follows the empirical relationship with average molecular weight per backbone bond M_b proposed by Fetters et al. on the basis of data for many random α-olefin copolymers. Master curves of storage modulus data provided evidence of large composition fluctuations and of mesophase separation transition at temperatures well above the melting point. Increasing the octene content of the soft blocks and lowering the temperature enhance the occurrence of MST, while increasing the CSA level moves the system toward a random copolymer structure thus suppressing MST. Within the range of parameters investigated, octene content has a larger effect on MST than CSA level (or block length). High-octene resins show MST even at high temperatures. Creep measurements made it possible to study terminal behavior. The octene content of the soft blocks increases the zero-shear viscosity and decreases the plateau modulus, while the total octene content increases the activation energy defined by eq 2. The CSA level decreases the activation energy but has little effect on the plateau modulus. Rheological and X-ray data showed that R09, with the highest octene content in its soft blocks, has a lamellar structure in the molten state.

Acknowledgment. This work was supported by The Dow Chemical Company and the National Science Foundation, Polymers Program (DMR-0505940 and DMR-1003942, to R.A.R.). The authors gratefully acknowledge Brian Landes (Dow) for stimulating discussions and for assistance with the SAXS measurements, conducted at DND-CAT at the Advanced Photon Source (APS). DND-CAT is supported by E.I. DuPont de Nemours & Co., The Dow Chemical Company and the State of Illinois. Use of the APS was supported by the U.S. Department of Energy, Office of Science, Office of Basic Energy Sciences, under Contract No. DE-AC02-06CH11357. HEP benefited from technical discussions with Dr. Si Wan Li at McGill University and thank Prof. M. Kamal at McGill University for the use of the PVT instrument.

References and Notes

(1) Hadjichristidis, N., Pispas, S., Floudas, G. A. *Block Copolymers*; Wiley-Interscience: Hoboken, NJ, 2003.
(2) Hamley, I. W. *Developments in Block Copolymer Science and Technology*; John Wiley & Sons: New York, 2004.
(3) Leibler, L. *Macromolecules* **1980**, *13*, 1602–1617.
(4) Adams, J. L.; Quiram, D. J.; Graessley, W. W.; Register, R. A.; Marchand, G. R. *Macromolecules* **1996**, *29*, 2929–2938.
(5) Rubinstein, M.; Obukhov, S. P. *Macromolecules* **1993**, *26*, 1740–1750.
(6) Coates, G. W.; Hustad, P. D.; Reinhartz, S. *Angew Chem Int Ed.* **2002**, *41*, 2236–2257.
(7) Coates, G. W.; Waymouth, R. M. *Scicnce* **1995**, *267*, 217–219.
(8) Dekmezian, A. H.; Soares, J. B. P.; Jiang, P.; García −Franco, C. A.; Weng, W.; Fuitwala, H.; Sun, T.; Sarzotti, D. M. *Macromolecules* **2002**, *35*, 9586–9594.
(9) Arriola, D. J.; Carnahan, E. M.; Hustad, P. D.; Kuhlman, R. L.; Wenzel, T. T. *Science* **2006**, *312*, 714–719. See also Supporting Online Material.
(10) Shan, C. L. P.; Hazlitt, L. G. *Macromol. Symp.* **2007**, *257*, 80–93.
(11) Khariwala, D. U.; Taha, A.; Chum, S. P.; Hiltner, A.; Baer, E. *Polymer* **2008**, *49*, 1365–1375.
(12) Li, S.; Register, R. A.; Landes, B. G.; Hustad, P. D.; Weinhold, J. D. *Macromolecules* **2010**, *43*, 4761–4770.
(13) Wang, H. P.; Khariwala, D. U.; Cheung, W.; Chum, S. P.; Hiltner, A.; Baer, E. *Macromolecules* **2007**, *40*, 2852–2862.
(14) Dias, P.; Lin, Y. J.; Poon, B.; Chen, H. Y.; Hiltner, A.; Baer, E. *Polymer* **2008**, *49*, 2937–2946.
(15) Wang, H.; Taha, A.; Chum, S. P.; Hiltner, A.; Baer, E. *Annu. Tech. Conf.* (*ANTEC*), *Soc. Plastics Eng.* **2009**, 1186–1190.
(16) Kamdar, A. R.; Wang, H. P.; Khariwala, D. U.; Taha, A.; Hiltner, A.; Baer, E. *J. Polym. Sci: Part B: Polym. Phys.* **2009**, *47*, 1554–1572.
(17) Hustad, P. D.; Marchand, G. R.; Garcia-Meitin, E. I.; Roberts, P. L.; Weinhold, J. D. *Macromolecules* **2009**, *42*, 3788–3794.
(18) Chum, P. S.; Swogger, K. W. *Prog. Polym. Sci.* **2008**, *33*, 797–819.
(19) Kempe, R. *Chem.—Eur. J.* **2007**, *13*, 2764–2773.
(20) Hustad, P. D.; Kuhlman, R. L.; Arriola, D. J.; Carnahan, E. M.; Wenzel, T. T. *Macromolecules* **2007**, *40*, 7061–7064.
(21) Nojima, S.; Kato, K.; Yamamoto, S.; Ashida, T. *Macromolecules* **1992**, *25*, 2237–2242.
(22) Rangarajan, P.; Register, R. A.; Fetters, L. J. *Macromolecules* **1993**, *26*, 4640–4645.
(23) Rangarajan, P.; Register, R. A.; Fetters, L. J.; Bras, W.; Naylor, S.; Ryan, A. J. *Macromolecules* **1995**, *28*, 4932–4938.
(24) Kofinas, P.; Cohen, R. E. *Macromolecules* **1995**, *28*, 336–343.
(25) Ryan, A. J.; Hamley, I. W.; Bras, W.; Bates, F. S. *Macromolecules* **1995**, *28*, 3860–3868.
(26) Sakurai, K.; MacKnight, W. J.; Lohse, D. J.; Schulz, D. N.; Sissano, J. A.; Lin, J.-S.; Agamalyan, M. *Polymer* **1996**, *37*, 4443–4453.
(27) Loo, Y. -L.; Register, R. A.; Ryan, A. J. *Macromolecules* **2002**, *35*, 2365–2374.
(28) Florez, S.; Muñoz, M. E.; Santamaria, A. *J. Rheol.* **2005**, *49*, 313–325.
(29) Honerkamp, J.; Weese, J. *Rheol. Acta* **1993**, *32*, 65–73.
(30) Ferry, J. D. *Viscoelastic Properties of Polymers*, 3rd ed.; John Wiley & Sons, Inc.: New York, 1980; pp 13, 29, 61, 64, 372.
(31) Gray, A. P. *Thermochim. Acta* **1970**, *1*, 563–579.
(32) Stühn, B. *J. Polym. Sci., Part B: Polym. Phys. Ed.* **1992**, *30*, 1013–1019.
(33) Soenen, H.; Liskova, A.; Reynders, K.; Berghmans, H.; Winter, H. H.; Overbergh, N. *Polymer* **1997**, *38*, 5661–1565.
(34) Bates, F. S. *Macromolecules* **1984**, *17*, 2607–2613.
(35) Dealy, J. M.; Larson, R. G. *Molecular Structure and Rheology of Molten Polymers*; Hanser Publishers: Munich, 2006; pp 150−155.
(36) Liu, C.; He, J.; van Ruymbeke, E.; Keunings, R.; Bailly, C. *Polymer* **2006**, *47*, 4461–4479. (N.B. These authors use the alternative definition of the plateau modulus.).
(37) Wu, S. *J. Polym. Sci., Part B: Polym. Phys.* **1989**, *27*, 723–741.
(38) García-Franco, C. A.; Harrington, B. A.; Lohse, J. J. *Macromolecules* **2006**, *39*, 2710–2717.
(39) Fetters, L. J.; Lohse, D. J.; García-Franco, C. A.; Brant, P.; Richter, D. *Macromolecules* **2002**, *35*, 10096–10101.
(40) Fetters, L. J.; Lohse, D. J.; Richter, D.; Witten, T. A.; Zirkel, A. *Macromolecules* **1994**, *27*, 4639–4647.
(41) Lohse, D. *J. Macromol. Sci.: Polym. Rev.* **2005**, *45*, 289–303.
(42) Kossuth, M. B.; Morse, D. C.; Bates, F. S. *J. Rheol.* **1999**, *43*, 167–196.
(43) Sebastian, J. M.; Graessley, W. W.; Register, R. A. *J. Rheol.* **2002**, *46*, 863–879.
(44) Morrison, F. A.; Winter, H. H. *Macromolecules* **1989**, *22*, 3533–3540.
(45) Williams, M. L.; Landel, R. F.; Ferry, J. D. *J. Am. Chem. Soc.* **1955**, *77*, 3701–3707.
(46) Rosedale, J. H.; Bates, F. S. *Macromolecules* **1990**, *23*, 2329–2338.
(47) Han, C. D.; Kim, J.; Kim, J. K. *Macromolecules* **1989**, *22*, 383–394. Han, C. D.; Baek, D. M.; Kim, J. K. *Macromolecules* **1990**, *23*, 561–570.
(48) Almdal, K.; Bates, F. S.; Mortensen, K. *J. Chem. Phys.* **1992**, *96*, 91222–9132.
(49) Bates, F. S.; Rosedale, J. H.; Fredrickson, G. H. *J. Chem. Phys.* **1990**, *92*, 6255–6270.
(50) Fredrickson, G. H.; Helfand, E. *J. Chem. Phys.* **1988**, *89*, 5890–5897.
(51) Kawasaki, K.; Onuki, A. *Phys. Rev. A* **1990**, *42*, 3664–3666.
(52) Matsen, M. W.; Schick, M. *Macromolecules* **1994**, *27*, 7157–7163.
(53) Kannan, R. M.; Kornfield, J. A. *Macromolecules* **1994**, *27*, 1177–1186.
(54) Lee, H. H.; Register, R. A.; Hajduk, D. A.; Gruner, S. M. *Polym. Eng. Sci.* **1996**, *36*, 1414–1424.
(55) Li, S.; Register, R. A.; Landes, B. G.; Hustad, P. D.; Weinhold, J. D. *Macromolecules* **2010**, *43*, 4761–4770.
(56) Khan, S. A.; Larson, R. G. *Rheol. Acta* **1991**, *30*, 1–6.
(57) Loo, Y.-L.; Register, R. A.; Ryan, A. J.; Dee, G. T. *Macromolecules* **2001**, *34*, 8968–8977.
(58) Hashimoto, T.; Nagatoshi, K.; Todo, A.; Hasegawa, H.; Kawai, H. *Macromolecules* **1974**, *7*, 364–373.